Range Extension Control System of Electric Vehicle Based on Optimal Torque Distribution and Cornering Resistance Minimization

Hiroshi Fujimoto and Hayato Sumiya
The University of Tokyo
5-1-5, Kashiwanoha, Kashiwa, Chiba, 227-8561 Japan
Email: fujimoto@k.u-tokyo.ac.jp, sumiya@hflab.k.u-tokyo.ac.jp

***Abstract*—Recently, electric vehicles (EVs) have received substantial attention. However, EVs have several problems that prevent their widespread use. In particular, the cruising distance per charge is the most important parameter. In order to solve the problem of a short cruising range, there have been many efforts to improve battery capacity. In contrast, in this paper, range extension control systems (RECSs) are proposed to enhance the efficiency based only on control technologies. Two types of range extension control systems are introduced, and their effectiveness is confirmed by experiments.**

I. Introduction

Nowadays, hybrid vehicles (HVs) and electric vehicles (EVs) are receiving attention because of environmental problems such as global warming, the exhaustion of fossil fuels, and air pollution. In particular, the environmental performance of EVs is superior to that of HVs because their greenhouse gases emissions are zero. In addition, EVs driven by electric motors have four advantages [1]. First, the development of in-wheel motors enables the individual control of each wheel. Second, continuous and smooth braking torque can be generated by regeneration. Third, the generated torque can be measured precisely from the motor current. Finally, quick torque response is available by motor current control. These advantages help to achieve effective vehicle motion control. Therefore, our research group has studied slip ratio control based on quick torque response and vehicle motion control by using the left and right driving force difference [2][3].

EVs have several advantages in terms of environmental performance as well as vehicle motion control. However, the use of EVs leads to several technical problems that prevent them from becoming widely used. Three of the problems that are often encountered are as follows. First, EVs are more expensive than internal combustion engine vehicles (ICEVs). Second, there are very few charging facilities for EVs. Finally, the cruising distance per charge is very short. In particular, the mileage per charge is insufficient. In order to solve this problem, several research efforts were undertaken to enhance the motor efficiency. A variable-parameter permanent-magnet motor was developed in [4] that can change magnetic flux according to the speed. Moreover, a novel drive method of the motor was proposed in [5], where the motor is driven with high efficiency by two reduction gears. However, to solve this problem definitively, it is generally believed that an improvement of the battery capacity is necessary.

In contrast, our research group has been developing range extension control systems (RECSs) to enhance the cruising range of EVs by control technologies. Here, "range" refers to the cruising range, which is the distance that can be traveled at a set speed for each charge of the vehicle. Two types of RECS have already been proposed. One is the efficiency optimization from an electric source to the motor output, which is called RECS-I [6]. The other is the efficiency optimization from the motor output to the translational speed and the yaw rate and is called RECS-II [7]. We assumed that an EV has more than one motor and that efficiency improvement is enabled by torque distribution.

If an EV has more than one motor, the sum of the torques generated by each motor only needs to satisfy the demands of the driver. Therefore, the torque values for each motor have several degrees of freedom. RECS-I improves the overall efficiency by controlling the driving and braking force of each motor.

RECS-II assumes that an EV has an active front steering system installed with electric power steering (EPS) or steer-by-wire (SbW). In the conventional method, when the vehicle is running on a curving road, a yaw moment is generated by the front steering angle only. However, the front steering angle generates not only the yaw moment but also the cornering resistance. In the proposed method, the yaw moment is generated by the front steering angle and the torque difference between the left and right motors. The proposed method can reduce the front steering angle, because the yaw moment, which is generated by the torque difference between the left and right motors, is also used. Therefore, the cornering resistance is reduced by the proposed method. As a result, the efficiency improves when the vehicle is speeding on a curving road.

In this paper, two types of range extension control systems are introduced, and the efficiency of the proposed method is evaluated by experiments.

II. Experimental vehicle

An original experimental EV "FPEV2-Kanon," which was developed in our laboratory, is used for performance verification. In this section, the characteristics of the experimental

(a) FPEV2-Kanon

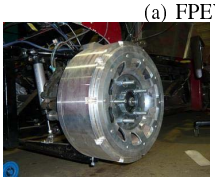

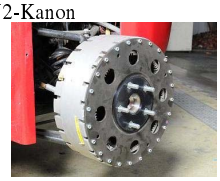

(b) Front in-wheel motor (c) Rear in-wheel motor

Fig. 1. Experimental vehicle.

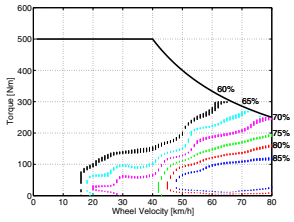

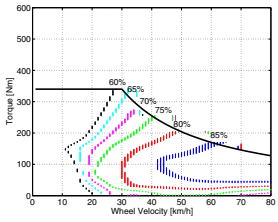

(a) Front motor. (b) Rear motor.

Fig. 2. Motor and inverter efficiency characteristics.

TABLE I
SPECIFICATION OF IN-WHEEL MOTORS.

	Front	Rear
Maximum/Rated Torque	500/110 [Nm]	340/137 [Nm]
Maximum/Rated Power	20.0/6.0 [kW]	10.7/4.3 [kW]
Rated Speed	300 [rpm]	382 [rpm]
Maximum Speed	1113 [rpm]	1500 [rpm]

vehicle are explained. Four in-wheel motors, which are of the outer-rotor type, are installed in each wheel (Table I). Since this motor uses a direct drive system, the reaction force from the road is directly transferred to the motor without gear reduction and backlash. Different efficiency motors are installed in the front and rear wheels. It is also possible to generate a yaw moment by using different driving forces between the left and right in-wheel motors. The steering mechanism adopts an active front and rear steering system, by using two 250 W DC motors as electric power steering (EPS). Moreover, to switch the steer-by-wire (SbW) and EPS systems, the steering wheel shaft has a removable structure.

Figure 1(a) shows the experimental vehicle, Fig. 1(b) and Fig. 1(c) show the front and rear in-wheel motors, respectively.

III. RANGE EXTENSION CONTROL SYSTEM BASED ON OPTIMAL TORQUE DISTRIBUTION (RECS-I)

A. Efficiency maps of the motors

We measured the motor efficiency maps used in this research. Figure 2 shows the measurements for both the front and rear wheel motors. The results are obtained from the inverter input to the motors' mechanical output. Then, the inverter efficiency and the line loss were also included. In addition, the mechanical output was obtained from the motor torque, which can be calculated from the current.

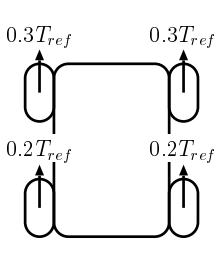

Fig. 3. Example of torque distribution.

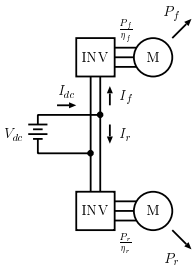

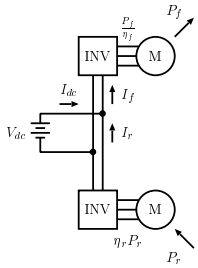

(a) Front drive rear drive. (b) Front drive rear regeneration.

Fig. 4. Driving patterns.

The complete efficiency maps with respect to the motor speed and torque are illustrated in Fig. 2. For electric vehicles with independent driven wheels, it is known that the motor efficiency changes significantly according to the operation points. In general, the speeds of the four wheels are almost the same when the car maintains a constant speed. In contrast, the torque of each motor can be set to a different value to achieve the optimal operation point in real time as long as the total torque matches the driver's requirement.

B. Constraints and overall efficiency

Here, an EV is assumed to move on a straight road and the torque is equally distributed between the left and right wheels to avoid yaw moment generation. As shown in Fig. 3, the torque can be distributed among the front and rear wheels, while the torque difference between the left and right wheels is kept zero. Therefore, this study is not only applicable to independent four-wheel drive vehicles, but can also be utilized for vehicles with two driving motors and independent front and rear wheel drive functions.

By using the proposed method, the front torque T_f and rear torque T_r can be determined with the help of the torque distribution rate ν. From (1) to (5), the total torque can fulfill the driver's required torque T_{ref} with arbitrary values of ν.

$$T_{ref} = T_f + T_r \quad (1)$$
$$T_f = T_{fl} + T_{fr} \quad (2)$$
$$T_r = T_{rl} + T_{rr} \quad (3)$$
$$T_f = (1-\nu)\, T_{ref} \quad (4)$$
$$T_r = \nu T_{ref} \quad (5)$$

Here T_{fl}, T_{fr}, T_{rl}, and T_{rr} are the front left wheel torque, front right wheel torque, rear left wheel torque, and rear right wheel torque, respectively. Moreover, the motor output power can be represented by the torque distribution ratio ν, the motor torque, and the motor angular velocity as

$$P_o = T_{ref}\omega_o = (T_f + T_r)\,\omega_o, \quad (6)$$
$$P_f = (1-\nu)\, P_o, \quad (7)$$
$$P_r = \nu P_o. \quad (8)$$

P_o, P_f, and P_r are the total motor output power, the front motor power, and the rear motor power, respectively. ω_o is the motor angular velocity, which is determined from the vehicle speed. Here, the wheel slip is assumed to be negligible. Finally,

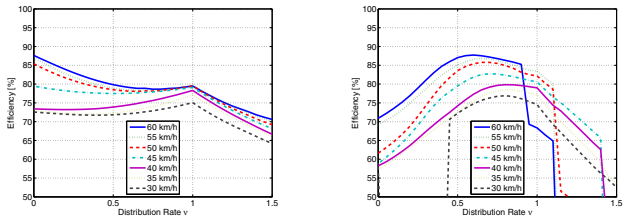

(a) $T_{ref} = 20$ [Nm] (b) $T_{ref} = 180$ [Nm]

Fig. 5. Torque distribution results to total torque reference.

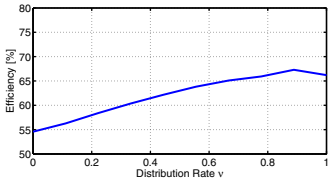

Fig. 6. Efficiency in experiments.

the overall efficiency η_{all} can be defined by the ratio between the motor output power and the battery output power as

$$\eta_{all} = \frac{\text{Motor output}}{\text{Electric sorce output}}. \tag{9}$$

C. Front and rear wheel motoring

Figure 4(a) shows the energy flow when the vehicle is driven by all wheels and all the necessary energy is supplied by the battery. In this case, the overall efficiency η_{all} is expressed as

$$\eta_{all} = \frac{P_f + P_r}{\frac{P_f}{\eta_f} + \frac{P_r}{\eta_r}} = \frac{\eta_f \eta_r}{(1-\nu)\eta_r + \nu\eta_f}. \tag{10}$$

D. Front wheel motoring and rear wheel regeneration

During acceleration, when the efficiency of each motor shows a large difference, it may be possible to improve the overall efficiency by combining motoring and regenerating operations. Although this scenario is factually unrealistic, we have to investigate this situation as a part of the basic research. Figure 4(b) shows the energy flow of a front-motoring and rear-regenerating vehicle. The energy for motoring is provided both by the regeneration and the battery. In this case, the overall efficiency η_{all} can be expressed by (11). Note that P_r is negative ($P_r < 0$) during regeneration.

$$\eta_{all} = \frac{P_f + P_r}{\frac{P_f}{\eta_f} + \eta_r P_r} = \frac{\eta_f}{1 - \nu + \nu\eta_f\eta_r} \tag{11}$$

E. Efficiency characteristics based on experimental motor

Efficiency maps of the motors used in the experimental vehicle are shown in Fig. 2. The simulation plots are shown in Fig. 5, which is based on (10) and (11) with a torque distribution ratio ν from 0 to 1.5. In the simulation, $\nu = 0$ implies only a front wheel drive and $\nu = 1.0$ implies only a rear wheel drive. Moreover, $\nu = 1.5$ indicates the situation when the rear wheel torque is 1.5 times the total torque command, and this is achieved by the negative torque of the front wheel.

TABLE II
CRUISING RANGE (KM) PER INPUT ENERGY (1 KWH) (RECS-I).

ν	0	0.5	0.88	1
km/kWh	3.2	3.6	4.1	3.8

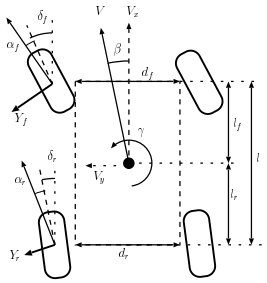

Fig. 7. Vehicle model.

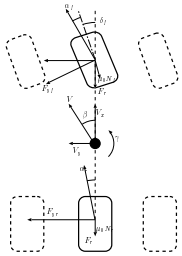

Fig. 8. Two-wheel model.

From Fig. 5(b), it is observed that the efficiency drops sharply and this can be explained by Fig. 2, in which the maximum torque decreases along with the increase in the motor speed. The total efficiency cannot be calculated by the torque limiter in the large ν^* range, as shown in Fig. 5(b). In addition, it is understood from Fig. 5(b) that the optimal ν exists in the range 0.4 to 0.9 at the large torque reference ($T_{ref} = 180$ [Nm]). Using the same calculations as those shown in Fig. 5, the optimal distribution ratio ν^* can be determined by the given total torque reference and the vehicle speed in real time. Hence, by using this optimal torque distribution map of the front and rear wheels, the cruising range can be extended.

F. Experiment

The experiment is conducted at a speed of 30 km/h, and the total torque command is set to 180 Nm. Experimental results are shown in Fig. 6. The overall efficiency varied according to the torque distribution ratio ν.

The cruising range per unit input energy (1 kWh) is evaluated based on these experiments. The battery output energy E is calculated by the integral calculation of the battery power $V_{dc}I_{dc}$ with the measurement time t. Then, in the same manner, the driving distance L is obtained by the integral of the motor speed with the same measurement time t. Therefore, by dividing E by L, the cruising range (km) per input energy (1 kWh) can be obtained. The results are listed in Table II, and 30% improvement can be achieved by comparing the worst and the best cases. In other words, the mileage is extended by 30% per charge. For example, the MISTUBISHI MOTORS i-MiEV [8] has a battery capacity of approximately 16 kWh. This improvement corresponds to a 14 km range extension based on the above calculation.

IV. RANGE EXTENSION CONTROL SYSTEM BASED ON CORNERING RESISTANCE MINIMIZATION (RECS-II)

A. Vehicle modeling

1) Vehicle dynamics: In this section, vehicle dynamics with a four-wheel drive and front and rear steering is explained [9].

Figure 7 shows the vehicle model. The lateral motion and yaw-dynamics are represented by

$$F_y = MV\left(\dot{\beta}+\gamma\right) = F_{yfl}+F_{yfr}+F_{yrl}+F_{yrr}, \quad (12)$$

$$M_z = I\dot{\gamma} = F_{yfl}l_f + F_{yfr}l_f - F_{yrl}l_r - F_{yrr}l_r + \frac{d_f}{2}\left(-F_{xfl}+F_{xfr}\right) + \frac{d_r}{2}\left(-F_{xrl}+F_{xrr}\right), \quad (13)$$

where F_y is the lateral force, M_z is the yaw-moment at the vehicle center of gravity, F_{yfl}, F_{yfr}, F_{yrl} and F_{yrr} are the lateral forces generated by each wheel, M is the vehicle mass, β is the vehicle side-slip angle, γ is the yaw-rate, and I is the vehicle yaw inertia. l_f and l_r are the distances from the body center of gravity to the steering knuckle spindle, and rear-wheel axle, respectively. d_f and d_r are the tread bases of the front and rear axle, respectively.

Wheel side-slip angles are the angles between the wheel traveling direction and the wheel rotation direction. These are represented by α_{fl}, α_{fr}, α_{rl}, and α_{rr}, respectively.

If the left and right tire characteristics are the same and the front and rear steering angles are small, the lateral forces generated by the left and right tire can be regarded as equal. In this condition, the relations between the wheel side-slip angles and the lateral forces are represented by

$$\alpha_{fl} \simeq \alpha_{fr} \simeq \alpha_f = \beta + \frac{l_f\gamma}{V} - \delta_f, \quad (14)$$

$$\alpha_{rl} \simeq \alpha_{rr} \simeq \alpha_r = \beta - \frac{l_r\gamma}{V} - \delta_r, \quad (15)$$

$$F_{yfl} \simeq F_{yfr} \simeq F_{yf} = -C_f\alpha_f, \quad (16)$$

$$F_{yrl} \simeq F_{yrr} \simeq F_{yr} = -C_r\alpha_r, \quad (17)$$

where F_{yf} and F_{yr} are the front and rear lateral forces, respectively, V is the vehicle velocity, and C_f and C_r are the cornering stiffness.

2) Driving resistance: In this section, the driving resistance is explained. This occurs by front steering when a vehicle is running on a curving road. Figure 8 shows a simplified bicycle model. This model assumes that the left and right tire characteristics are the same. Tires generate lateral forces and rolling friction when the vehicle is moving. Longitudinal elements of these forces and disturbances, such as the wind and the road condition, become the driving resistance F_r. The driving resistance F_r is represented by

$$F_r = 2F_{yf}\sin\delta_f + \mu_0 N_f\cos\alpha_f + \mu_0 N_r\cos\alpha_r + F_{dis}, \quad (18)$$

where F_{dis} represents disturbances such as the wind and the road slope, μ_0 is the rolling friction coefficient, and N_f and N_r are the front and rear vertical forces.

B. Distribution method based on least square method

1) Cost function: Next, the cost function is defined to minimize the total loss. In this section, it is assumed that a rear-wheel-drive vehicle has a front active steering unit. Therefore, the front driving force and rear steering angle are regarded as 0. Thus, the power loss, which becomes the cost function, can be derived. The power loss P, which is generated by the EV, consists of three elements: mechanical output P_m, copper loss P_c, and iron loss P_i:

$$P = P_m + P_c + P_i. \quad (19)$$

Here, the iron loss P_i is ignored for the sake of simplicity. The mechanical output is calculated by the product of the torque and wheel speed. It is assumed that the torque is controlled by the $i_d = 0$ control and the copper loss is generated in proportion to the square of the q axis current i_q of the permanent magnetic motor:

$$P_m = T_{rl}\omega_{rl} + T_{rr}\omega_{rr} \quad (20)$$

$$P_c = R_{arl}i_{qrl}^2 + R_{arr}i_{qrr}^2, \quad (21)$$

where i_{qrl} and i_{qrr} are the q axis currents of the left and right motors, and R_{arl} and R_{arr} are the armature winding resistance of the left and right rear motors, respectively.

It is assumed that all the wheels adhere to the road. The driving force and yaw-moment are realized by the left and right motors. In addition, the left and right armature winding resistances and torque constants are assumed to be equal because the same motors are installed in the left and right rear wheels. The mechanical output and the copper loss are represented by

$$P_m = F_xV_x + N_z\gamma, \quad (22)$$

$$P_c = \frac{R_a r^2}{K_t^2}\left(\frac{1}{2}F_x^2 + \frac{2}{d_r^2}N_z^2\right), \quad (23)$$

where F_x is the driving force, N_z is the yaw moment generated by the torque difference between the left and right motors, and K_t is the motor torque constant [7]. The sum of (22) and (23) gives the total power loss.

A public road typically consists of straight and curving sections. Moreover, curving sections can be regarded as a series of circles with different radii. Therefore, in this paper, it is assumed that the vehicle is in steady circle turning with a constant velocity and a constant yaw rate. The driving force needs the same value of driving resistance to be maintained to turn with constant velocity. The mechanical output and copper loss are represented as (24) and (25) by substituting (18) for (22) and (23) when the vehicle is moving on a curve.

$$P_m = \left(2F_{yf}\sin\delta_f + \mu_0 N_z\cos\delta_f + \mu_0 N_r\right)V_x + N_z\gamma \quad (24)$$

$$P_c = \Big(\frac{R_a r^2}{2K_t^2}\big(2F_{yf}\sin\delta_f + \mu_0 N_z\cos\delta_f + \mu_0 N_r\big)^2 + \frac{2R_a r^2}{K_t^2 d_r^2}N_z^2\Big) \quad (25)$$

2) Distribution method: The lateral motion (12) and the yaw-dynamics (13) are re-formulated as

$$\begin{bmatrix} -2C_f & -2C_r & 0 \\ -2C_f l_f & 2C_r l_r & 1 \end{bmatrix}\begin{bmatrix} \alpha_f \\ \alpha_r \\ N_z \end{bmatrix} = \begin{bmatrix} F_y \\ M_z \end{bmatrix}, \quad (26)$$

where the left-hand side coefficient matrix is defined as $\boldsymbol{A}$, and the vector of the wheel side-slip angles and the yaw-moment is defined as $\boldsymbol{x} = [\alpha_f \ \alpha_r \ N_z]^T$. The right-hand side vector

TABLE III
KM PER KWH (EXPERIMENTAL RESULTS).

Battery capacity	Without RECS	With RECS
1 kWh	8.03 km	8.20 km
16 kWh	128.61 km	131.23 km

$[F_y \ M_z]^T$ is defined as $\boldsymbol{b}$. The cost function J is derived as (27) under the assumption that the rolling friction is negligible and the front steering angle is approximated to be sufficiently small.

$$J = 2F_{yf}\delta_f V_x + N_z\gamma + \frac{2R_a r^2}{K_t^2}F_{yf}^2\delta_f^2 + \frac{2R_a r^2}{K_t^2 d_r^2}N_z^2 \quad (27)$$

J is minimized by the distribution of the front and rear wheel side-slip angle and the yaw-moment generated by the torque difference. Therefore, it is necessary that the front steering angle δ_f be represented by the front and rear wheel side-slip angles α_f and α_r. The front steering angle δ_f is represented by substituting (14) for (15).

$$\delta_f = \frac{l}{V}\gamma - (\alpha_f - \alpha_r) \quad (28)$$

In addition, the yaw rate γ of the lateral motion (12) is substituted for (28). In this paper, the time derivative of the vehicle side-slip angle β is assumed to be zero because steady circle turning is assumed. Then, from (12), yaw-rate γ is represented by

$$\gamma = \frac{-2C_f\alpha_f - 2C_r\alpha_r}{MV}. \quad (29)$$

Equation (30) is derived from (16), (28), and (29).

$$\begin{aligned} J \simeq & \left(\frac{4C_f^2 l}{MV} + 2C_f V\right)\alpha_f^2 + \left(\frac{4C_f C_r l}{MV} - 2C_f V\right)\alpha_f\alpha_r \\ & - \frac{2C_f}{MV}\alpha_f N_z - \frac{2C_r}{MV}\alpha_r N_z + \frac{2R_a r^2}{K_t^2 d_r^2}N_z^2 \end{aligned} \quad (30)$$

In this paper, α_f^4, $\alpha_f^2\alpha_r^2$, $\alpha_f^2 N_z$, and $\alpha_f\alpha_r N_z$ are regarded as small enough and these values are ignored. Then, the minimization becomes possible by a least square method.

In addition, $\boldsymbol{W}$ is defined as the weighting matrix. The weighted least square solution $\boldsymbol{x_{opt}}$ is represented by

$$J = \boldsymbol{x}^T\boldsymbol{W}\boldsymbol{x}, \quad (31)$$

$$\boldsymbol{x_{opt}} = \boldsymbol{W}^{-1}\boldsymbol{A}^T\left(\boldsymbol{A}\boldsymbol{W}^{-1}\boldsymbol{A}^T\right)^{-1}\boldsymbol{b}, \quad (32)$$

$$\boldsymbol{W} = \begin{bmatrix} \frac{4C_f^2}{MV}l + 2C_f V & \frac{2C_f C_r}{MV}l - C_f V & \frac{-C_f}{MV} \\ \frac{2C_f C_r}{MV}l - C_f V & 0 & \frac{-C_r}{MV} \\ \frac{-C_f}{MV} & \frac{-C_r}{MV} & \frac{2r^2 R_a^2}{K_t^2 d_r^2} \end{bmatrix}. \quad (33)$$

The optimal solution is obtained as (32) to minimize J, which can satisfy the required conditions in terms of the given lateral force, yaw moment, and vehicle velocity. References of the front steering angle and left and right torques are generated by these values.

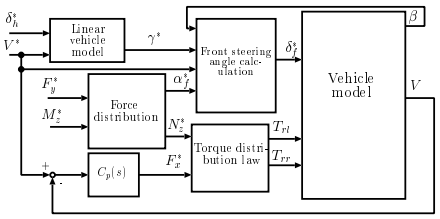

Fig. 9. Block diagram of the range extension control system.

C. Experiment

Figure 9 shows the block diagram of the proposed range extension control system. In the conventional method, the vehicle turns only the front steering angle. In the proposed method, the vehicle uses the front- and rear-wheel side-slip angles and the yaw-moment generated by the torque difference between the left and right motors, which are calculated by (32). Both the conventional and the proposed methods are verified using steady circle turning. These methods are compared by the sum of the mechanical output based on (20) and the copper loss based on (21). The vehicle velocity controller is designed to keep the velocity constant. The proportional gain in the vehicle velocity controller is designed by the pole placement method. A simple plant model is considered to design the vehicle velocity controller as

$$V = \frac{1}{Ms}F_x. \quad (34)$$

The closed-loop pole of the vehicle velocity controller is set to -5 rad/s. The vehicle velocity controller $C_p(s)$ corresponds to the driver model. The driving force controlled by $C_p(s)$ and the yaw-moment calculated with (32) are used to derive the left and right torque inputs. In this study, only the front-wheel side-slip angle (α_f) control is considered, because an experimental vehicle with front active steering is assumed. The reference of the front steering angle δ_f^* is calculated from α_f^* by

$$\delta_f^* = \beta + \frac{l_f\gamma^*}{V^*} - \alpha_f^*. \quad (35)$$

The vehicle velocity V^* in (35) is given from the vehicle velocity reference. The yaw rate γ^* is calculated by the vehicle linear model from the front steering angle δ_h^* and the vehicle velocity V^*[9]. δ_h^* is the front steering angle command of the human driver to turn the same radius circle by the conventional method without the torque difference in the yaw moment. Moreover, the vehicle side-slip angle β in (35) is assumed to be measurable. The reference of the lateral force F_y^*, which is used in the proposed method, is calculated from the circle radius, vehicle velocity, and vehicle mass. It is represented by

$$F_y^* = \frac{MV^2}{R}, \quad (36)$$

where R is the circle radius. The circle radius in which the vehicle is moving in the case of the conventional method is used. In addition, the reference of the yaw moment is $M_z^* = 0$. This is because the yaw-rate is constant. The

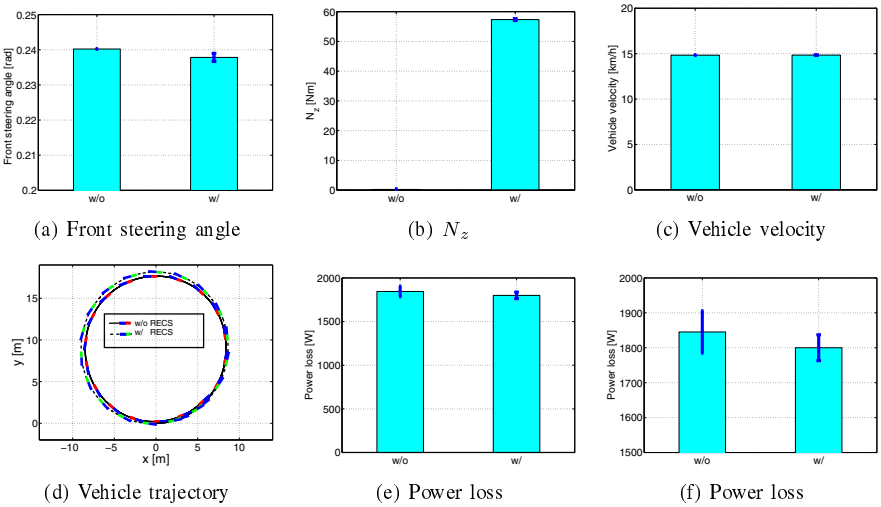

(a) Front steering angle (b) N_z (c) Vehicle velocity

(d) Vehicle trajectory (e) Power loss (f) Power loss

Fig. 10. Experimental results.

nominal values of the front- and rear-cornering stiffness are $C_f = 8000$ N/rad and $C_r = 15000$ N/rad, respectively. The experiments are carried out in a parking area that belongs to our university. The experimental conditions are as follows: vehicle velocity $V = 15$ km/h and circle radius $R = 8$ m. Both the conventional method and the proposed method are examined using steady circle turning. In the experiments, the power loss is measured from the product of the inverter input voltage V_{dc} and inverter input current I_{dc}. These results include not only the mechanical output and the copper loss but also the iron loss and the efficiency of the inverter and the motor. In order to confirm repeatability of the experimental results, 10 times the average values of both the conventional method and the proposed method are used. Moreover, the standard deviation $\pm\sigma$ of each result is shown as error bars.

Figure 10 shows the experimental results. The front steering angle is reduced, as shown in Fig. 10(a) and the torque difference in the yaw moment is generated by the proposed method, as shown in Fig. 10(b). It is confirmed that the torque difference compensates for the yaw rate with a smaller steering angle. Both the conventional and the proposed methods have the same velocity, as shown in Fig. 10(c). Figure 10(d) shows the vehicle trajectory. The vehicle trajectory for the proposed method is little larger than that for the conventional method. This is because the yaw rate is reduced slightly by the distribution. The power loss is reduced by almost 50 W in the proposed method as shown in Fig. 10(e) and Fig. 10(f). The power losses are calculated from the inverter input measurements. It is confirmed that the power loss is reduced by approcimately 3% in the proposed method.

Table III shows the cruising range (km) per input energy (1 kWh), which is calculated in a manner similar to that used in section III-F. It is extended to 200 m per 1 kWh, as given in Table III.

V. Conclusion

In this paper, range extension control systems are introduced and the advantages of the proposed methods are confirmed by experiments. Future work will combine the two proposed RECSs and consider the load transfer caused by acceleration.

Acknowledgment

This research was partly supported by the Industrial Technology Research Grant Program from the New Energy and Industrial Technology Development Organization (NEDO) of Japan and in part by the Ministry of Education, Culture, Sports, Science and Technology grant number 22246057.

References

[1] Y. Hori, "Future vehicle driven by electricity and control – research on four-wheel-motored "UOT electric march II"," *IEEE Trans. Industrial Electronics*, vol. 51, no. 5, pp. 954–962, 2004.

[2] T. Suzuki and H. Fujimoto, "Slip ratio estimation and regenerative brake control without detection of vehicle velocity and acceleration for electric vehicle at urgent brake-turning," in *The 11th IEEE International Workshop on Advanced Motion Control Proceedings*, pp. 273–278, 2010.

[3] H. Fujimoto and Y. Yamauchi, "Advanced motion control of electric vehicle based on lateral force observer with active steering," in *IEEE International Symposium on Industrial Electronics 2010 Proceedings*, pp. 3627–3632, 2010.

[4] K. Sakai, K. Yuki, Y. Hashiba, N. Takahashi, and K. Yasui, "Principle of the variable-magnetic-force memory motor," in *Proc. International Conference of Electrical Machines and Systems*, pp. 1–6, 2009.

[5] A. Sorniotti, M. Boscolo, A. Turner, and C. Cavallino, "Optimization of a 2-speed gear box for an electric vehicle," in *Proc. 10th International Symposium on Advanced Vehicle Control*, pp. 755–760, 2010.

[6] T. Suzuki and H. Fujimoto, "Proposal of range extension control system by drive and regeneration distribution based on efficiency characteristic of motors for electric vehicle," in *IEE of Japan Technical Meeting Record*, no. IIC-10-19, pp. 23–28, 2010, (in Japanese).

[7] H. Sumiya and H. Fujimoto, "Range extension control system for electric vehicle with active front steering and driving/braking force distribution on curving road," in *Proc. The 36th Annual Conference of the IEEE Industrial Electronics Society*, pp. 2823–2828, 2010.

[8] M. Kamachi, H. Miyamoto, and H. Yoshida, "Development of electric vehicle for on-road test," in *Proc. 8th International Symposium on Advanced Vehicle Control*, pp. 665–669, 2008.

[9] R. Rajamani, *Vehicle Dynamics and Control*. Springer Science & Business Media, 2006.